FREYA Report after Berkeley visit

Dorthea Gjestvang

January 2018

1   Introduction

Computational simulations are a vital part in the studies of physis today. Simulating physical experiments before conducting them can not only tells us what we might expect from a certain experiment, but it also acts as a quality check of physical models. Implementing theory and comparing computational yields to experimental results gives insight on wheter we have understood the process or not.

This is no different in the study of fission in nuclear physics. There are several computational codes trying to simulate the fission process. One of these codes is FREYA, developed at the Lawrence Livermore Laboratory in California [1]. In this report, I will in section 2.1 give an overview on how FREYA simulates fission events as a step-by-step process. Thereafter, I will in section 2.1.1 discuss some key parameters in FREYA that can be subject to user manipulation. Thereafter, I will study three different fission cases, the spontaneous fission of ^{252}Cf, the thermal neutron induced fission of ^{235}U and lastly the neutron induced fission of ^{239}Pufor a range of incoming neutron energies. The results are presented in section 4, and discussed in section 5. I will focus on why FREYA gives certain results, and discuss the physical explanation behind the results.

2   Theory: FREYA

FREYA is short for Fission Reaction Yield Algorithm, and it is a computer code that models fission of nuclei [1]. In a fission event in FREYA, the energy, angular momentum and of the fragments and the emmited photons and neutrons are calculated, and thus it is possible to look at different aspects of the fission process using the same model. The calculations in FREYA are based on experimental data [1], and today it can model spontaneous fission, photofission and neutron-induced fission of some given nuclei.

2.1   Fission event in FREYA

The simulation of a fission event in FREYA proceeds in several steps: pre-fission, during fission and post-fission, and I will focus on those aspects of the

process that are of the most importance for this report. FREYA only concider the fission event, and the neutron and gamma emission from the pre-equilibrium nucleus, the compound nucleus and the fission fragments, and it does not take into account further decay of the fission products.

First, FREYA concider the pre-equilibrium nucleus, and the chance for pre-equilibrium neutron emission. This is only significant for high energies [1]. Next, after the compound nucleus is equilibriated, the code concider pre-fission neutron evaporation, where a neutron is emmited before fission occurs. The resulting $A-1$-nuclei can either fission, or emit another neutron. As each resulting nuclei can either emit a pre-fission neutron or fission, this process is called multichance fission.

After pre-fission radiation, FREYA moves on to the fission process. Using a energy-dependent fission fragment distribution, the mass numbers of the two fragments are decided, and the charge is split in accordance to a gaussian probability distribution, where the peak corresponds to the fragments having the same fraction of charge to mass as the nucleus that fissions [1]. The total mass number A and the charge Z is conserved in the fission process.

Now the energies of the fission fragments are to be determined. FREYA relies on experimental data to input the total kinetic energy TKE of the fission fragments for a given compound nuclei excitation energy [1]. By calculating the Q-value of the fission reaction and subtracting the average TKE, the energy available as excitation energy for the two fragments is found. This energy is split between rotational and statistical excitation energy, and split between the two fragments. The total energy of the system is conserved.

The last part of the FREYA fission event is the post-fission radiation, which consist of neutron and photon emission. First, the fission fragments emit neutrons until their statistical excitation energy is below the neutron separation energy, and neutron emission is no longer possible. Then the photon emission starts, beginning as a statistical cascade of photons. First the statistical excitation energy of the fission fragment is disposed of, then when the statistical excitation energy drops below a givel limit g_{min}, the emission of photons conntinues, now exhausting the rotational energy of the nucleus. This is colllective, discrete transitions between theoretical rotational bands in the nucleus. At low energies the photon emission continues as discrete transitions, using data from the RIPL-3 library [1]. When the remaining excitation energy is belov the limit g_{min}, or the nucleus has an half-life longer than the limit t_{max}, the process stops.

2.1.1 Parameters in FREYA

There are several adjustable parameters in FREYA, that enables the user to fit the calculations to experimental results. I will focus on those that are important for this report.

As mentioned earlier, the total kinetic energy of the fragment TKE_{data} is needed as input in FREYA. FREYA further assumes that the avergage total kinetic energy takes the following form [1]:

$$\overline{TKE}(A_H, E_n) = \overline{TKE_{data}}(A_H) + dTKE(E_n) \tag{1}$$

dTKE is an adjustable parameter, used to reproduce the measured average neutron multiplicity ν [1]. As the excitation energy E is given by

$$E = Q - dTKE \tag{2}$$

where Q is the energy released in the fission process, the dTKE-parameter adjusts the ratio of kinetic enery and excitation energy in the nucleus.

The parameter c_s, called the spin temperature [1], adjusts the ratio between the fragment's rotational and statistical exitation energy. The angular momentum of the nucleus is drawn from a Boltzmann distribution, where c_s is the factor that determines the temperature of the Boltzmann distribution. For $c_s = 1$ the angular momentum is drawn from a thermal distribution, and the higher the c_s, the higher probability of nuclei with high angular momentum. Thus, the higher c_s, the less statistical excitation energy will the fragments get.

Observations show that statistical excitation energy is not shared evenly between the light and the heavy fission fragment, but rather that the lighter fragment is favoured [1]. After an initial energy division, where the statistical excitation energy is split between the two fragments in accordance to their heat capacities and the light fragment gets a statistical excitation energy E_L, the energy is shifted in favour of the light fragment by factor $x > 1$ in the following way:

$$E_L \rightarrow xE_L \tag{3}$$

A higher x will thus give the light frament a larger portion of the available statistical excitation energy.

3 Method

This report is based on simulations run with FREYA v2.0.3. Each case was run with 100000 iteratations, and with the default parameters provided by FREYA, unless otherwise specified.

The first case analysed was the spontaneous fission of ^{252}Cf. The dependence of the mean neutron multiplicity ν, the mean neutron multiplicity from the light and heavy fissions fragment ν_1 and ν_2, and the mean gamma multiplicity N_γ was studied under the change of the parameters dTKE, x and c_s. The fission fragment and product distribution was plotted. The neutron and photon multiplicity distribution, spectral shape and the angular correlation between pairs of emmited neutrons were also calculated.

Thereafter, the neutron induced fission of ^{235}U was studied, where the incoming neutron had an energy of $E_n = 0.1$ MeV. Again, the fission fragment and products were plotted, the neutron and photon multcity distributions and

spectral shapes calculated, and the angular correlation between pairs of emitted neutrons extracted.

The last case studied in this report, was the neutron-induced fission of ^{239}Pu for a range of different neutron energies. The effect of different neutron energies was studied when comparing the neutron and photon multiplicity distributions, the angular correlation between pair of emmited neutrons, and the fission fragment yields.

4 Results

4.1 Spontaneous fission of ^{252}Cf

The four first neutron factorial moments is shown in Table 1, and the dependence of the mean neutron multiplicity ν and the photon multiplicity N_γ on the parameters dTKE and x can be seen in Table 2 and 3 respectively. The dependence of N_γ on c_s is shown in Table 4.

The fragment and product mass distribution is shown in Figure 1, and the mean kinetic energy of the fragments as a function of mass is shown in Figure 2. The multiplicity distribution and spectral shape of the emmited neutrons and photons respectively is shown in Figure 3, 4, 5 and 6. The angular correlation between pairs of emmited neutrons are shown in Figure 7.

Table 1: The four first neutron factorial moments from the spontaneous fission of ^{252}Cf

Moment	Value
1	3.7490(61)
2	12.009(11)
3	32.130(18)
4	69.777(26)

Table 2: The dependence of $\overline{\nu}$ and $\overline{\nu_1}$, $\overline{\nu_2}$ and $\overline{N}_\gamma$ on dTKE, when x=1.27 is held constant

Variable	dTKE = 0.01	dTKE = 0.32	dTKE=0.52 (default)	dTKE= 1.00	dTKE= 1.52
$\overline{\nu}$	3.8087(62)	3.7740(61)	3.7490(61)	3.6883(61)	3.6274(60)
$\overline{\nu_1}$	2.2093(47)	2.1896(47)	2.1710(47)	2.1423(46)	2.1065(46)
$\overline{\nu_2}$	1.5994(40)	1.5844(40)	1.5779(40)	1.5460(39)	1.5209(40)
$\overline{N}_\gamma$	7.7066(88)	7.6707(88)	7.6826(88)	7.6687(88)	7.6553(87)

Table 3: The dependence of $\overline{\nu}$, $\overline{\nu_1}$, $\overline{\nu_2}$ and $\overline{N}_\gamma$ on x, when dTKE=0.52 is held constant

Variable	x = 0.80	x = 1.00	x = 1.27 (default)	x = 1.30	x= 1.40
$\overline{\nu}$	3.7489(61)	3.7725(61)	3.7490(61)	3.7465(61)	3.7115(61)
$\overline{\nu_1}$	1.3456(37)	1.7073(41)	2.1710(47)	2.2282(47)	2.3883(49)
$\overline{\nu_2}$	2.4032(49)	2.0652(45)	1.5779(40)	1.5182(39)	1.3232(36)
$\overline{N}_\gamma$	7.6394(87)	7.65454(87)	7.6826(88)	7.6911(88)	7.7025(88)

Table 4: The dependence of $\overline{N}_\gamma$ on c_s

	cs=0.77	cs= 0.82	cs=0.87 (default)	cs= 0.97	cs= 1.07
$\overline{N}_\gamma$	7.4015(86)	7.5337(87)	7.6826(88)	7.9506(89)	8.2386(91)
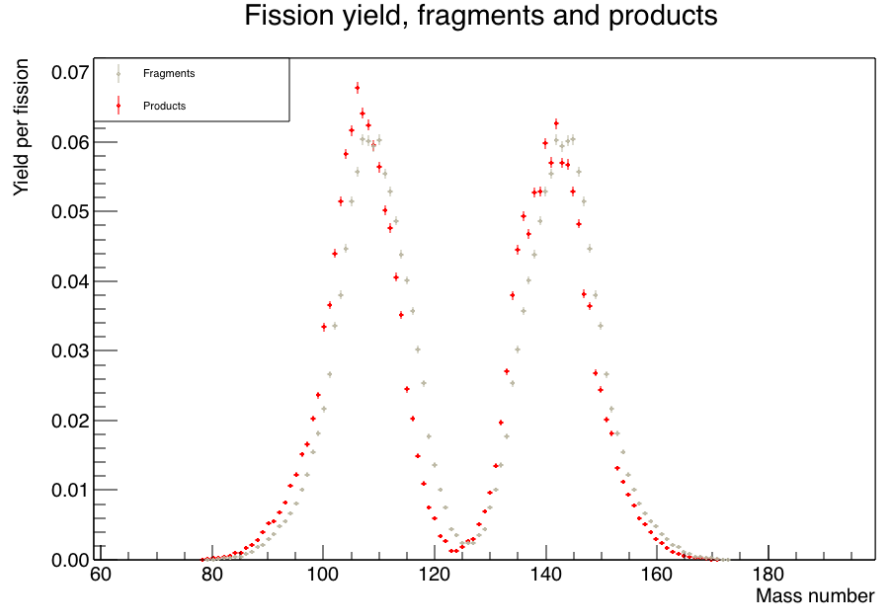
Figure 1: The fragment and product yield from the spontaneous fission of ^{252}Cf
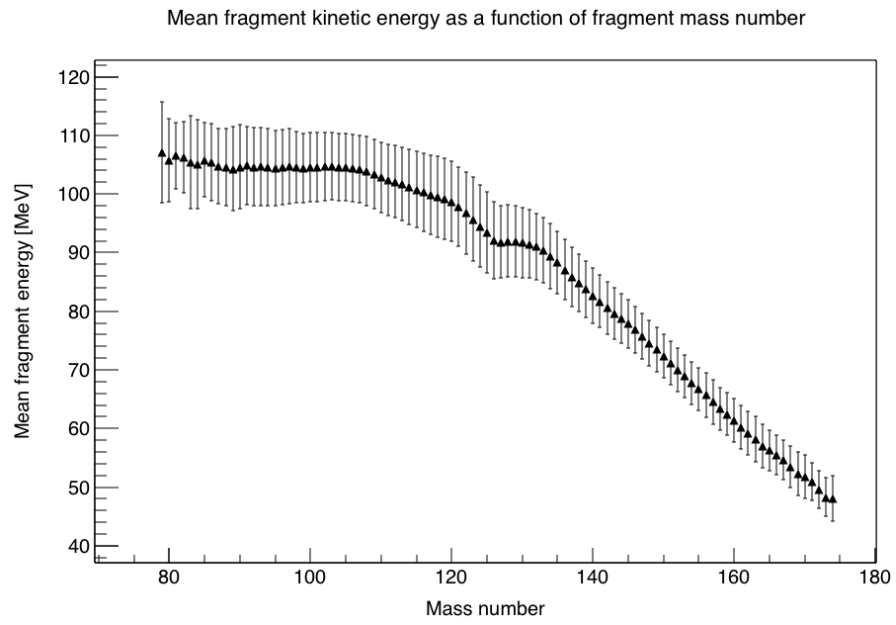
Figure 2: The mean fragment energy as a function of fragment mass, from the spontaneous fission of ^{252}Cf
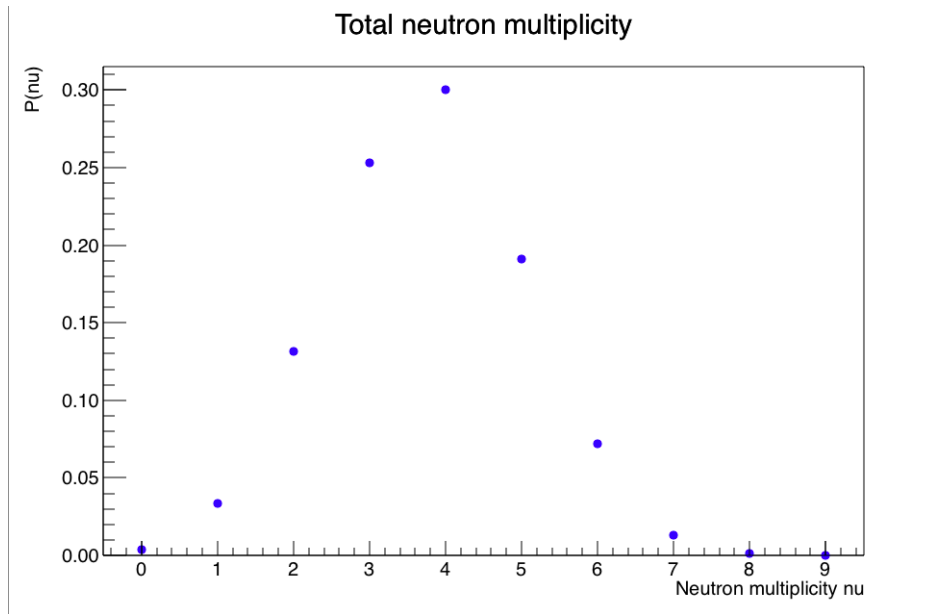
Figure 3: The multiplicity distribution of neutrons from the spontaneous fission of ^{252}Cf
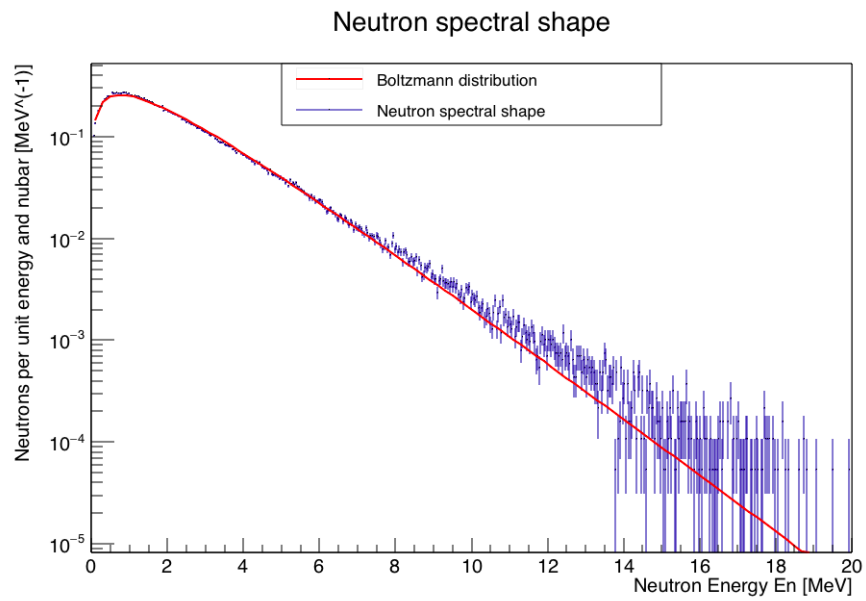
Figure 4: The spectral shape of neutrons from the spontaneous fission of ^{252}Cf, compared to a fitted Boltzmann distribution
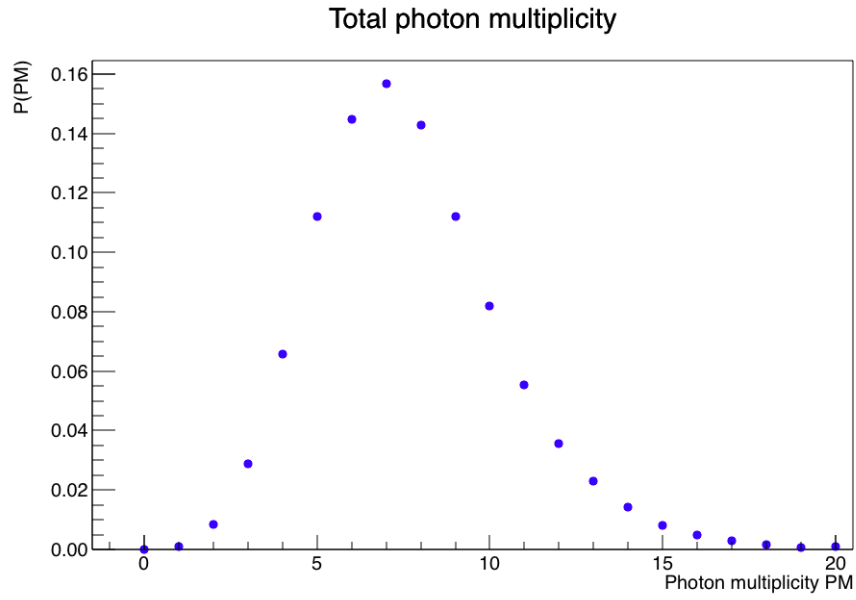
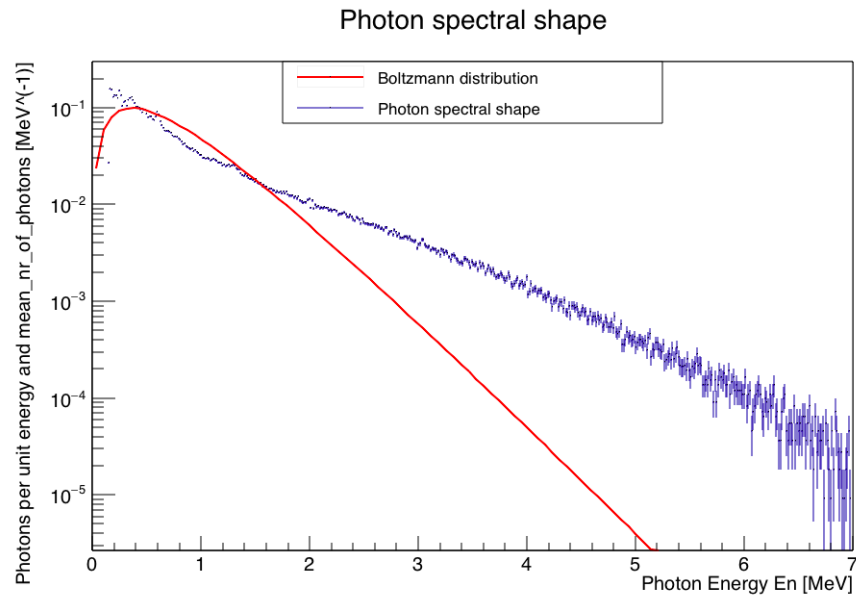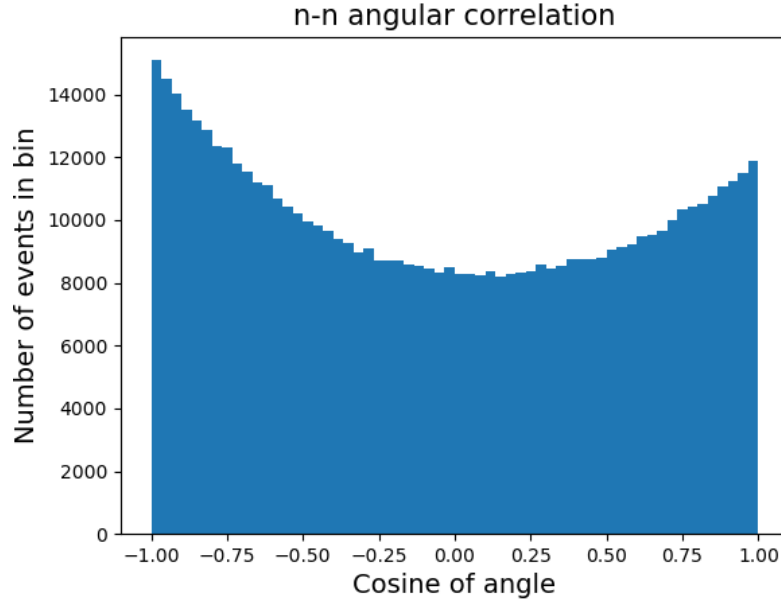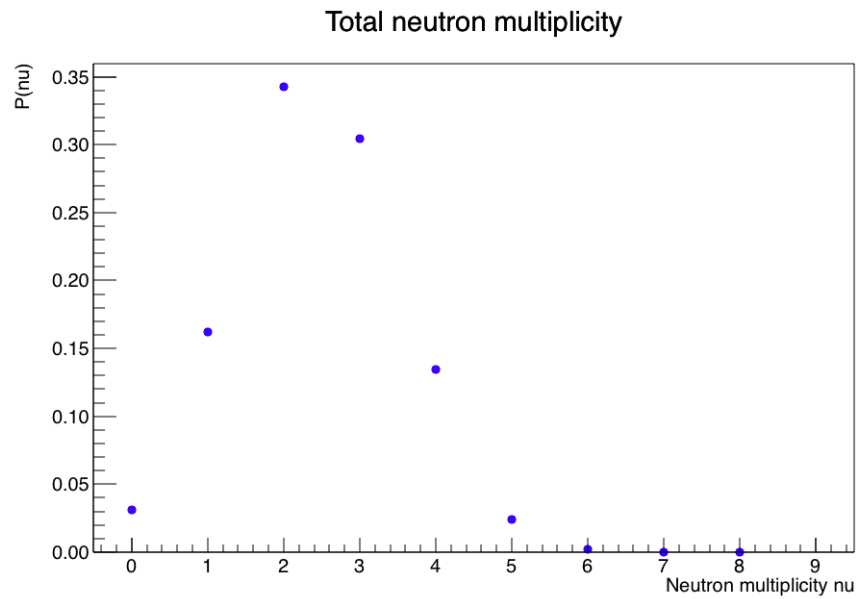Figure 5: The multiplicity distribution of photons from the spontaneous fission of ^{252}Cf

Figure 6: The spectral shape of photons from the spontaneous fission of ^{252}Cf, compared to a fitted Boltzmann distribution

8

Figure 7: The angulare correlation between pairs of emmited neutrons from the spontaneous fission of ^{252}Cf

4.2 Thermal neutron induced fission of ^{235}U

The four first neutron factorial moments is shown in Table 5. The fragment and product distribution is shown in Figure 8.

The multiplicity distribution and spectral shape of the emmited neutrons and photons respectively is shown in Figure 9, 10, 11 and 12. The angular correlation between pairs of emmited neutrons are shown in Figure 13.

Table 5: Neutrons, first four factorial moments, from thermal neutron-induced fission of ^{235}U

Moment	Value
1	2.4297(49)
2	4.6693(68)
3	6.7716(82)
4	7.0186(84)

9
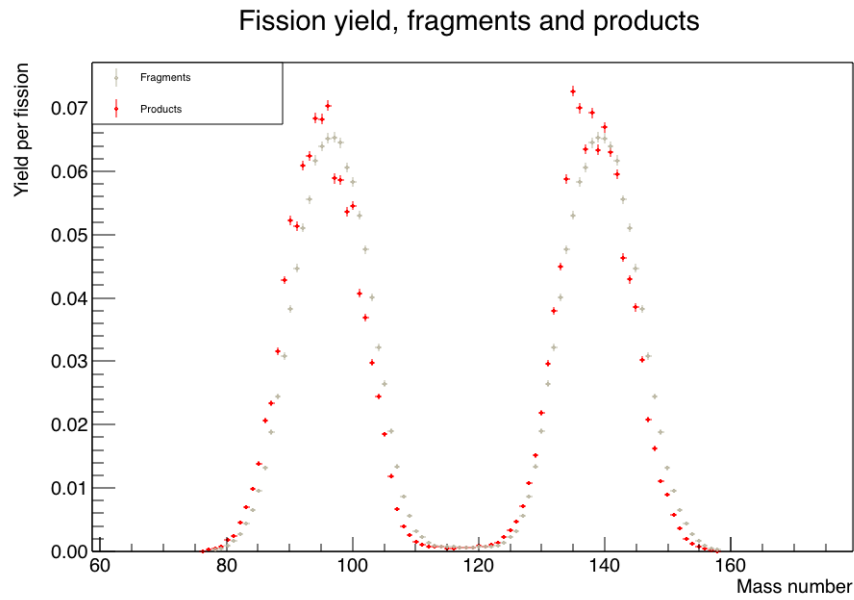
Figure 8: The fragment and product mass distribution from the thermal neutron induced fission of ^{235}U

Figure 9: The multiplicity distribution of neutrons from the thermal neutron-induced fission of ^{235}U
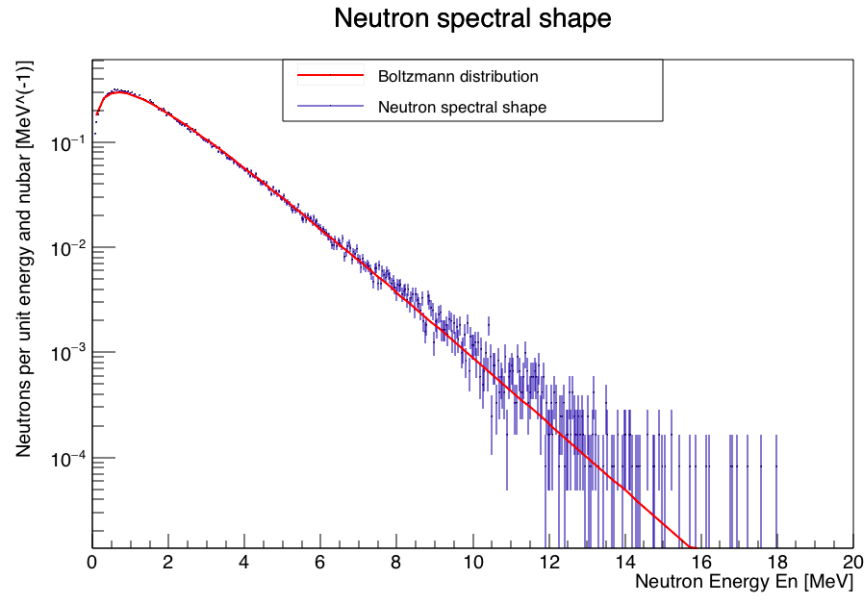
10

Figure 10: The spectral shape of neutrons from the thermal neutron induced fission of ^{235}U, compared to a fitted Boltzmann distribution
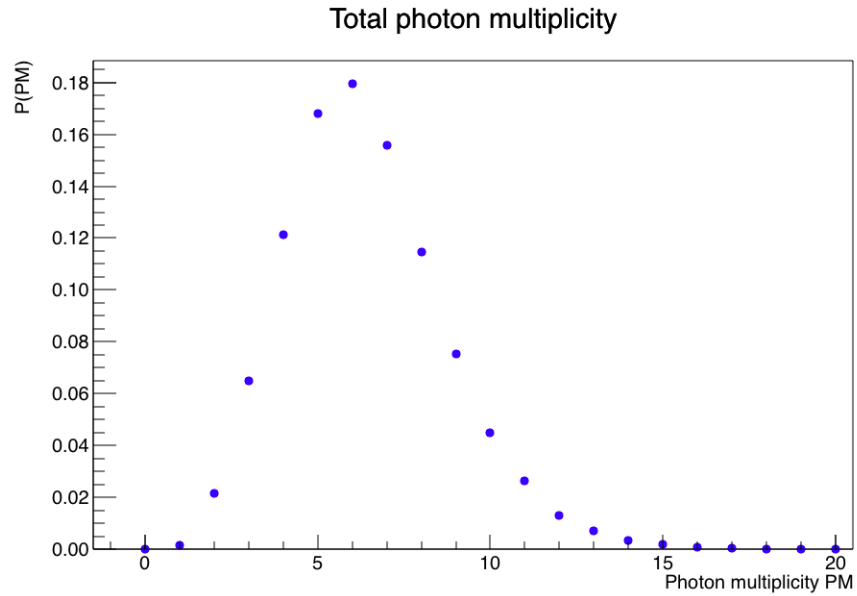

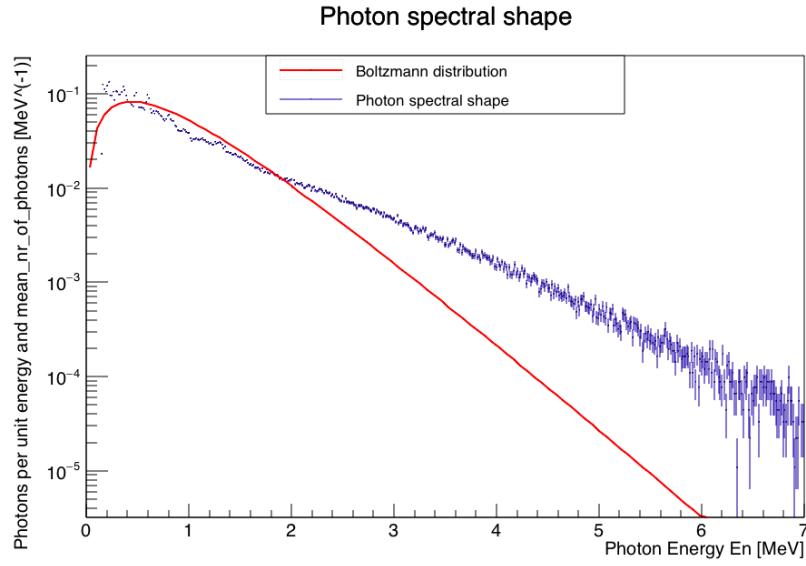Figure 11: The multiplicity distribution of photons from the thermal neutron-induced fission of ^{235}U

Figure 12: The spectral shape of photons from the thermal neutron induced fission of ^{235}U, compared to a fitted Boltzmann distribution
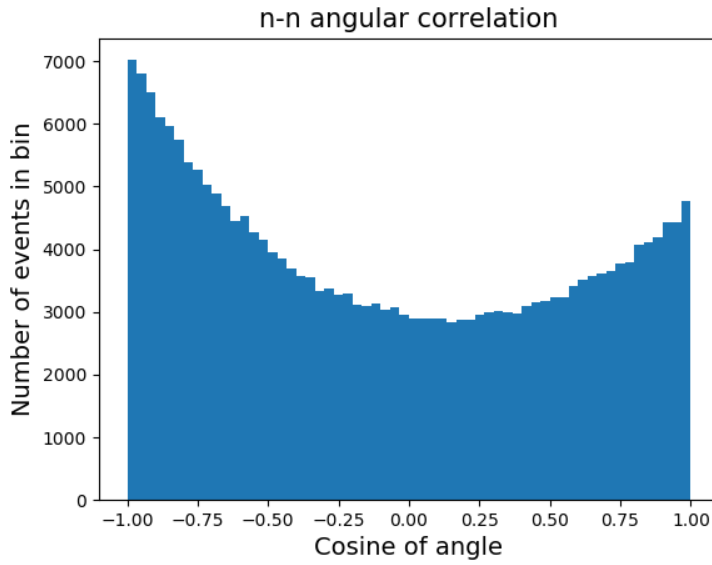

Figure 13: The angulare correlation between pairs of emmited neutrons from the thermal neutron-induced fission of ^{235}U

4.3 Neutron induced fission of ^{239}Pu

4.3.1 Neutron factorial moments for ^{239}Pu

The first four neutron factorial moments for the neutron induced fission of ^{239}Pu for incoming neutron energies $0.1, 2, 8, 14$ and 20 MeV can be seen in Table 6 - 10.

Table 6: Neutrons, first four factorial moments. From neutron-induced fission of ^{239}Pu, with $E_n = 0.1$ MeV

Moment	ν	ν_0	ν_1	ν_2
1	2.8903(54)	0.0000(00)	1.6201(40)	1.2702(36)
2	6.7476(81)	0.0000(00)	1.7531(42)	0.9778(31)
3	12.2142(11)	0.0000(00)	1.0750(33)	0.4033(20)
4	16.2727(13)	0.0000(00)	0.2986(17)	0.0694(83)

Table 7: Neutrons, first four factorial moments. From neutron-induced fission of ^{239}Pu, with $E_n = 2.0$ MeV

Moment	ν	ν_0	ν_1	ν_2
1	3.1397(56)	0.00338(18)	1.7466(42)	1.3913(37)
2	8.1242(90)	0.0000(00)	2.1249(46)	1.2498(35)
3	16.7641(13)	0.0000(00)	1.5852(40)	0.6584(26)
4	26.4527(16)	0.0000(00)	0.6012(25)	0.1807(13)

Table 8: Neutrons, first four factorial moments. From neutron-induced fission of ^{239}Pu, with $E_n = 8.0$ MeV

Moment	ν	ν_0	ν_1	ν_2
1	3.8262(62)	0.5467(23)	1.9769(44)	1.5760(40)
2	12.6219(11)	0.0000(00)	2.9383(54)	1.7681(42)
3	35.2788(19)	0.0000(00)	3.0971(56)	1.3733(37)
4	82.0861(29)	0.0000(00)	2.2596(48)	0.7162(27)

Table 9: Neutrons, first four factorial moments. From neutron-induced fission of ^{239}Pu, with $E_n = 14.0$ MeV

Moment	ν	ν_0	ν_1	ν_2
1	4.4980(67)	0.9311(30)	2.2991(48)	1.7334(42)
2	18.217(13)	0.4845(22)	4.3236(66)	2.2436(47)
3	65.9636(26)	0.0000(00)	6.5792(81)	2.1349(46)
4	212.075(46)	0.0000(00)	8.1756(90)	1.4522(38)

Table 10: Neutrons, first four factorial moments. From neutron-induced fission of ^{239}Pu, with $E_n = 20.0$ MeV

Moment	ν	ν_0	ν_1	ν_2
1	5.0461(71)	1.1136(33)	2.5768(51)	1.9135(44)
2	23.3884(15)	0.7220(27)	5.6124(75)	2.8325(53)
3	98.8097(31)	0.0416(64)	10.176(10)	3.1657(56)
4	377.024(61)	0.0000(00)	15.203(12)	2.5877(51)

4.3.2 Fragment and product mass distributions

The fragment and product distribution from the neutron-induced fission of ^{239}Pu for incoming neutron energies $E_n = 0.1$, 8 and 20 MeV is shown in Figure 14, 15, 16.
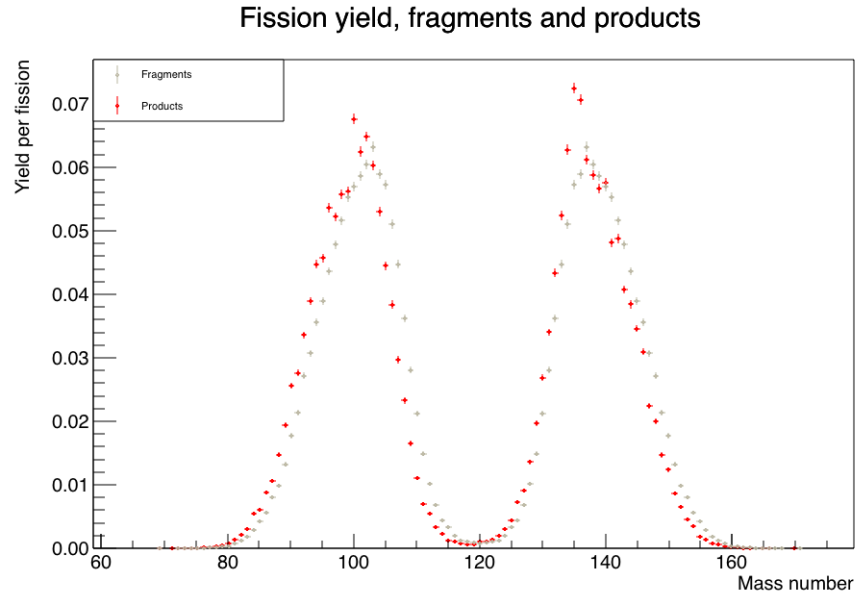
Figure 14: The fragment and product distribution from the neutron-induced fission of ^{239}Pu with $E_n = 0.1$ MeV
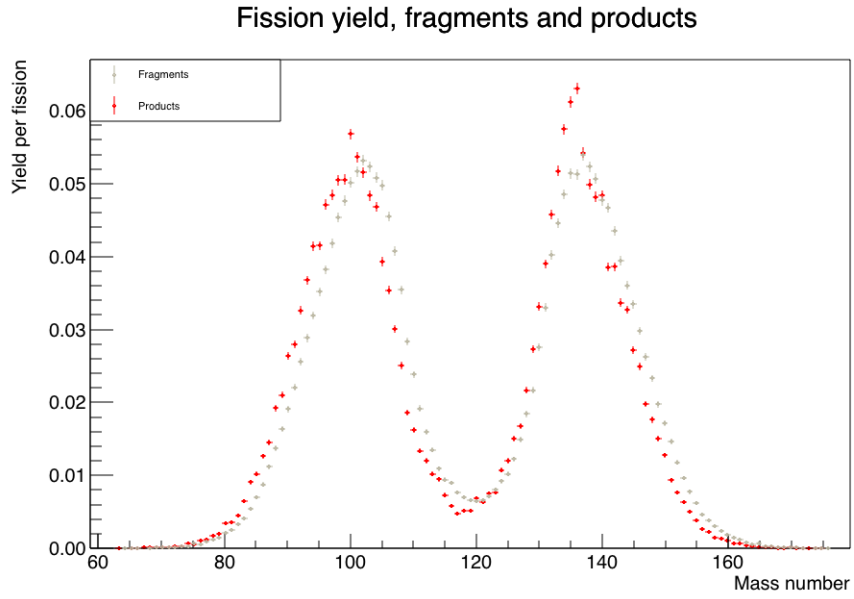

Figure 15: The fragment and product distribution from the neutron-induced fission of ^{239}Pu with $E_n = 8$ MeV
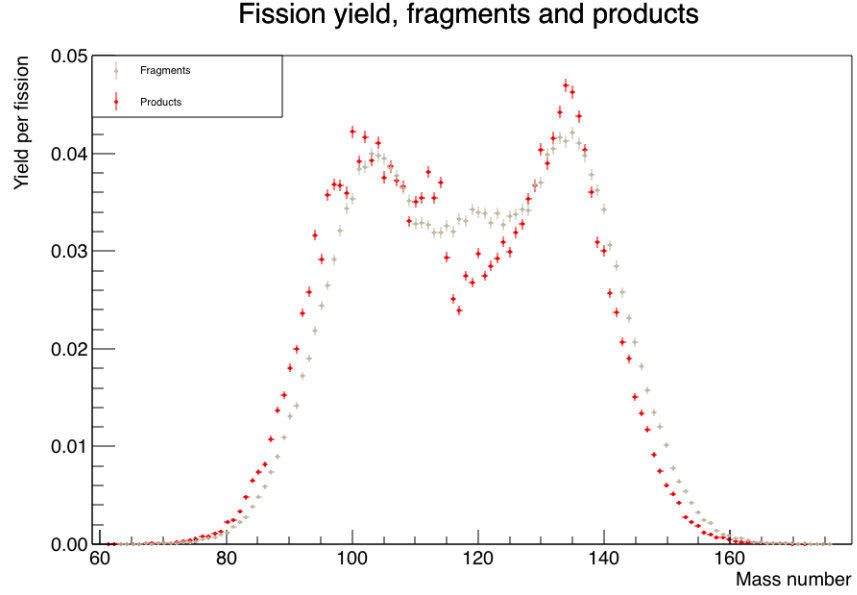
15

Figure 16: The fragment and product distribution from the neutron-induced fission of ^{239}Pu with $E_n = 20$ MeV

4.3.3 Neutron multiplicity distribution and spectral shape

The neutron multiplicity distribution for the neutron-induced fission of ^{239}Pu for the incoming neutron energies $E_n = 0.1$, 8 and 20 MeV is shown in Figure 17, 18 and 19.

The spectral shapes of the same incoming neutron energies are shown in Figure 20, 21 and 22.
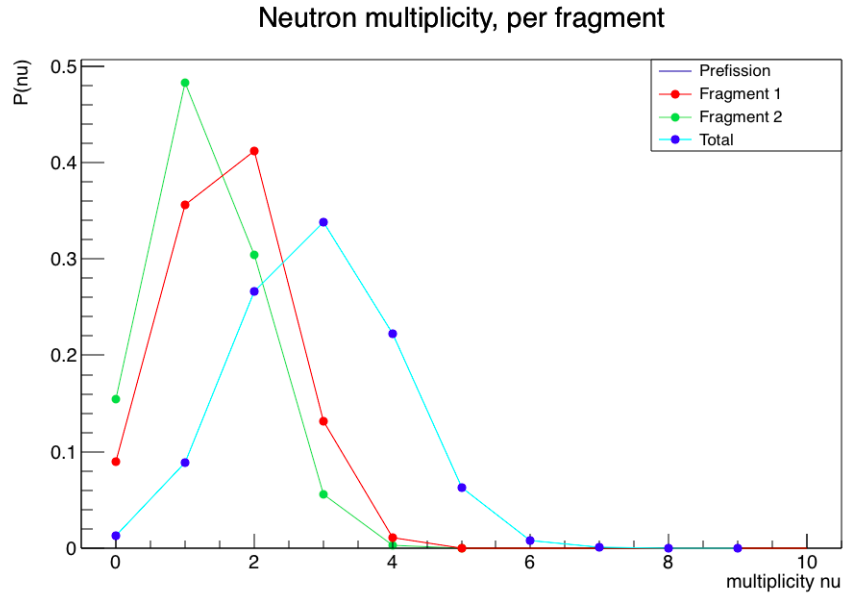
Figure 17: The neutron multiplicity distribution from the neutron-induced fission of ^{239}Pu with $E_n = 0.1$ MeV
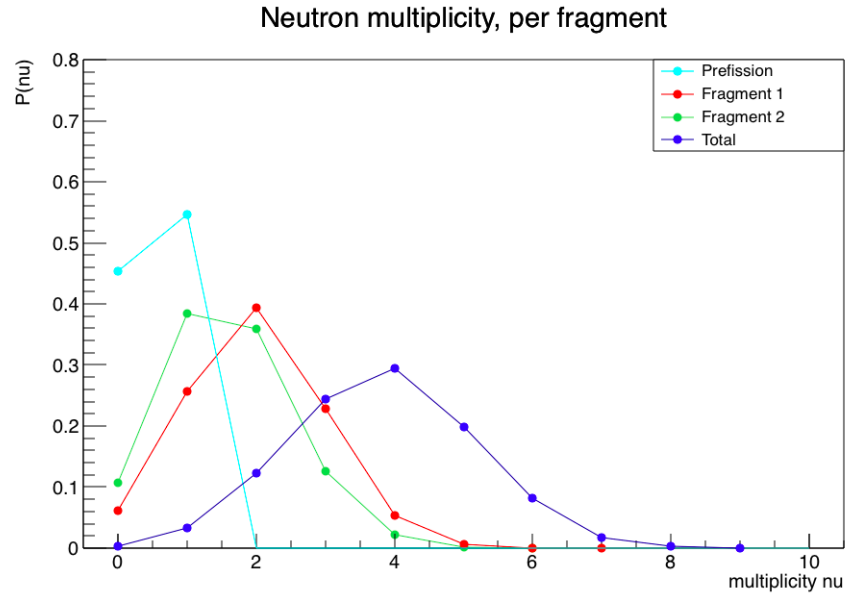
Figure 18: The neutron multiplicity distribution from the neutron-induced fission of ^{239}Pu with $E_n = 8$ MeV
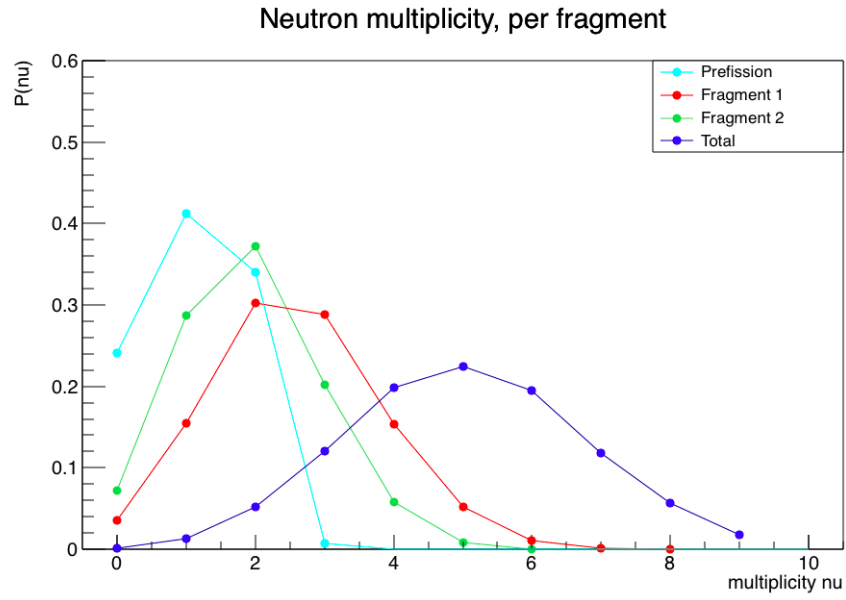
Figure 19: The neutron multiplicity distribution from the neutron-induced fission of ^{239}Pu with $E_n = 20$ MeV
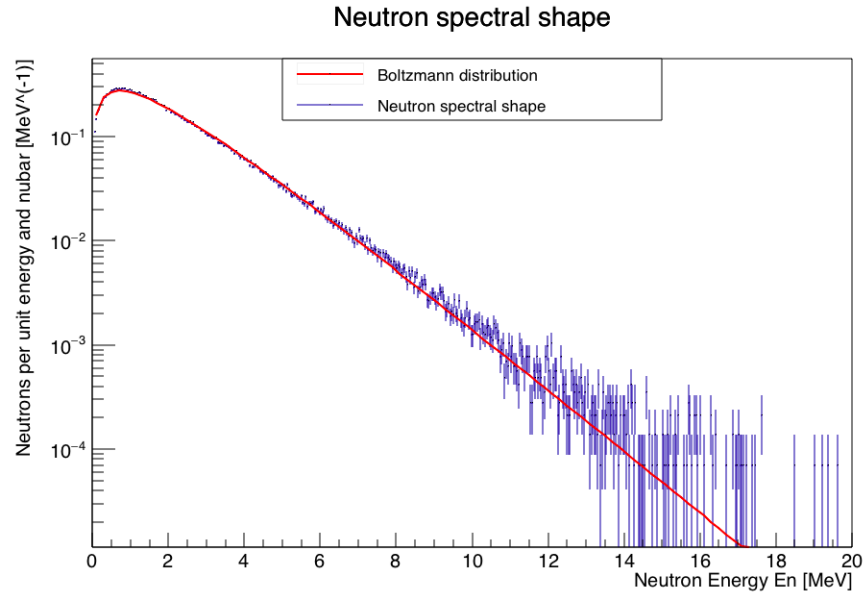

Figure 20: The neutron spectral shape from the neutron-induced fission of ^{239}Pu with $E_n = 0.1$ MeV, compared to a Boltzmnn distribution
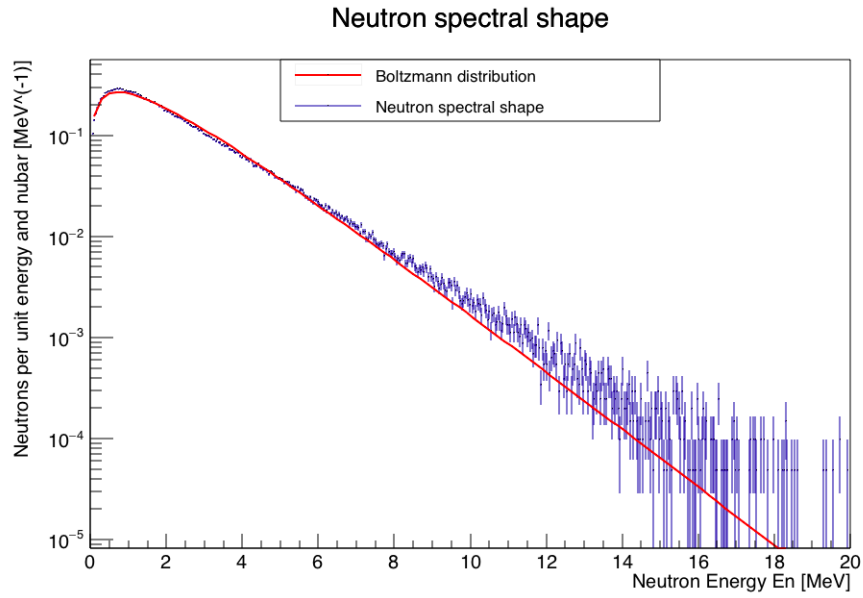
Figure 21: The neutron spectral shape from the neutron-induced fission of ^{239}Pu with $E_n = 8$ MeV, compared to a Boltzmnn distribution
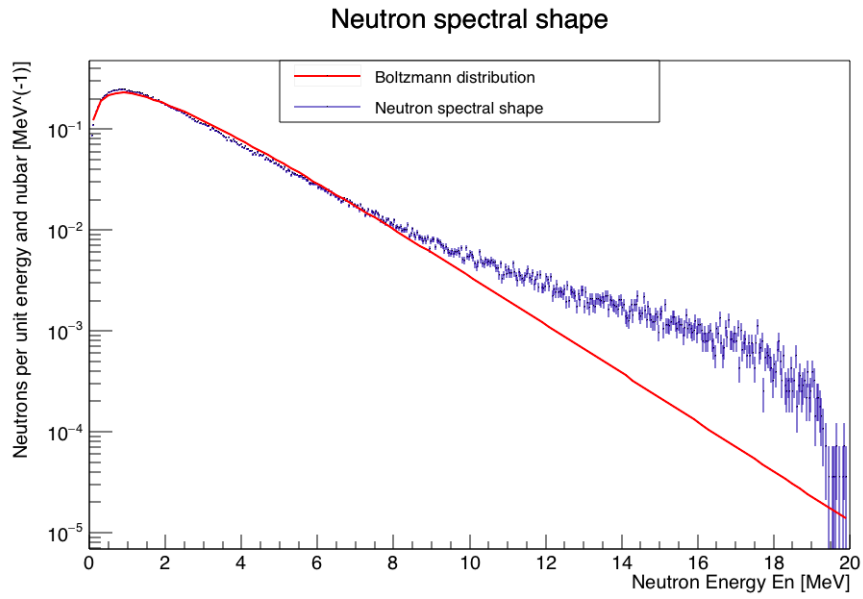

Figure 22: The neutron spectral shape from the neutron-induced fission of ^{239}Pu with $E_n = 20$ MeV, compared to a Boltzmnn distribution

4.3.4   Photon multiplicity distribution and spectral shape

The photon multiplicity distribution for the neutron-induced fission of ^{239}Pu for the incoming neutron energies $E_n = 0.1$, 8 and 20 MeV is shown in Figure 23, 24 and 25.

The spectral shapes of the same incoming neutron energies are shown in Figure 26, 27 and 28.
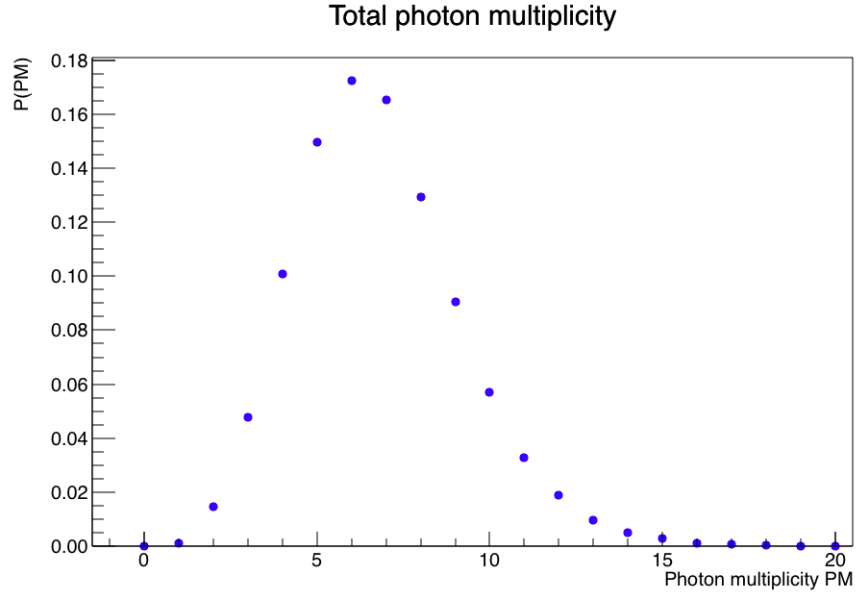
Total photon multiplicity

Figure 23: The photon multiplicity distribution from the neutron-induced fission of ^{239}Pu with $E_n = 0.1$ MeV
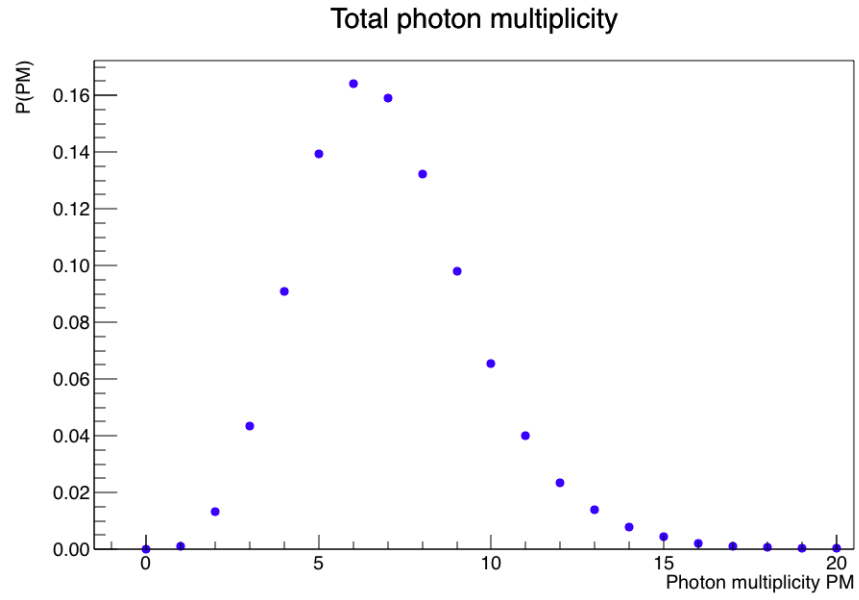
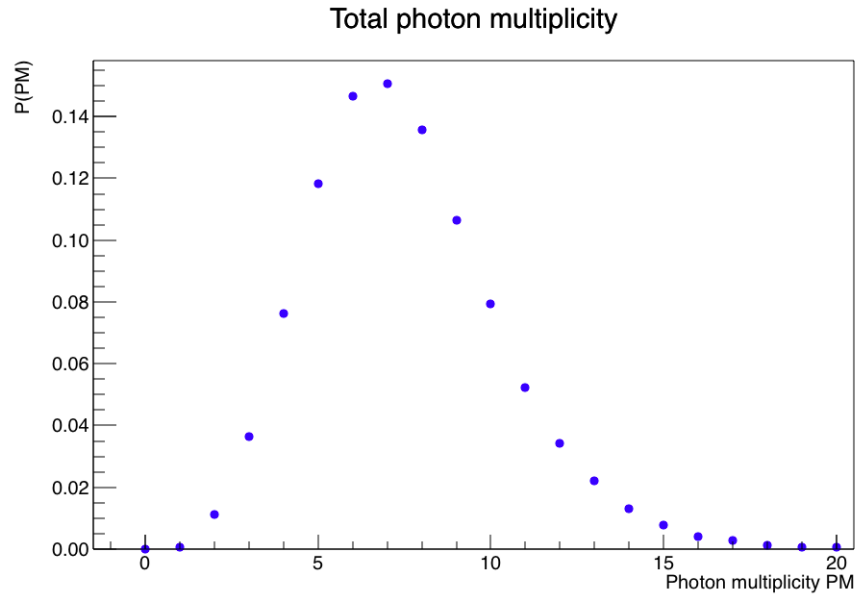Figure 24: The photon multiplicity distribution from the neutron-induced fission of ^{239}Pu with $E_n = 8$ MeV

Figure 25: The photon multiplicity distribution from the neutron-induced fission of ^{239}Pu with $E_n = 20$ MeV
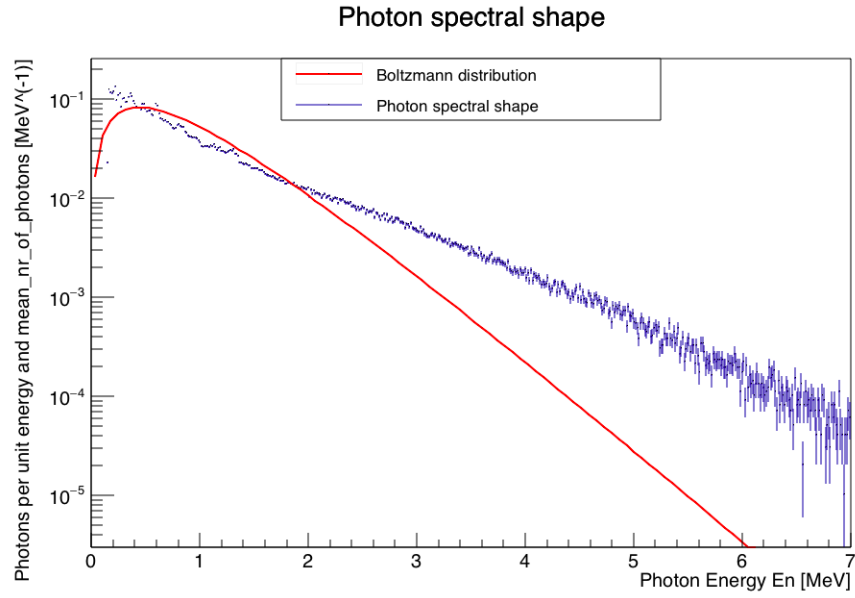
21

Figure 26: The photon spectral shape from the neutron-induced fission of ^{239}Pu with $E_n = 0.1$ MeV, compared to a Boltzmnn distribution
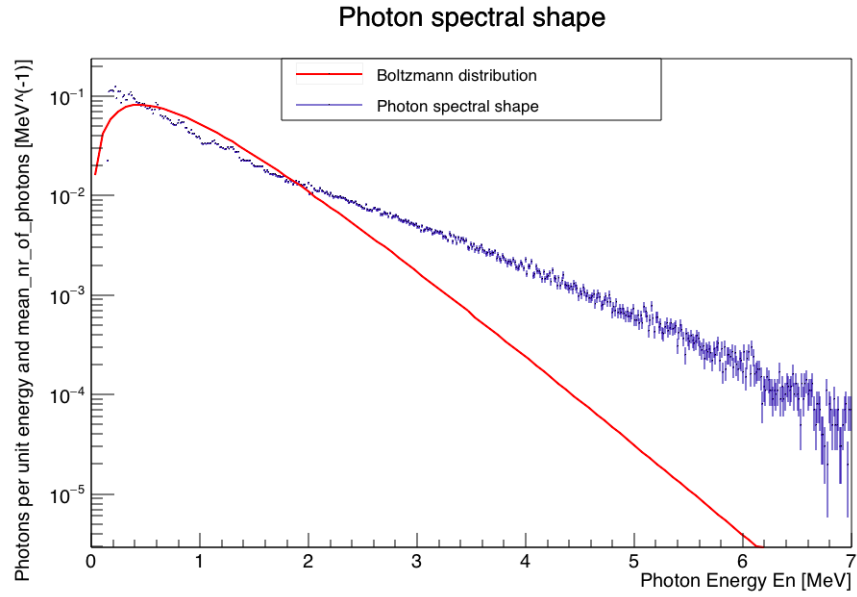

Figure 27: The photon spectral shape from the neutron-induced fission of ^{239}Pu with $E_n = 8$ MeV, compared to a Boltzmnn distribution

Figure 28: The photon spectral shape from the neutron-induced fission of ^{239}Pu with $E_n = 20$ MeV, compared to a Boltzmnn distribution
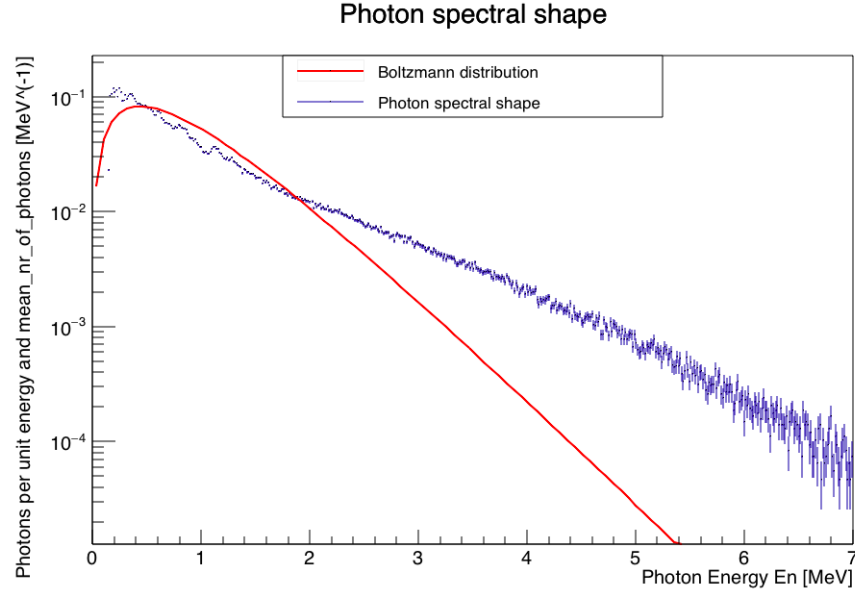
4.3.5 Angular correlation of neutron pairs

The angular correlation between pair of emmited neutrons for the incoming neutron energies $E_n = 0.1$, 8 and 20 MeV are shown in Figure
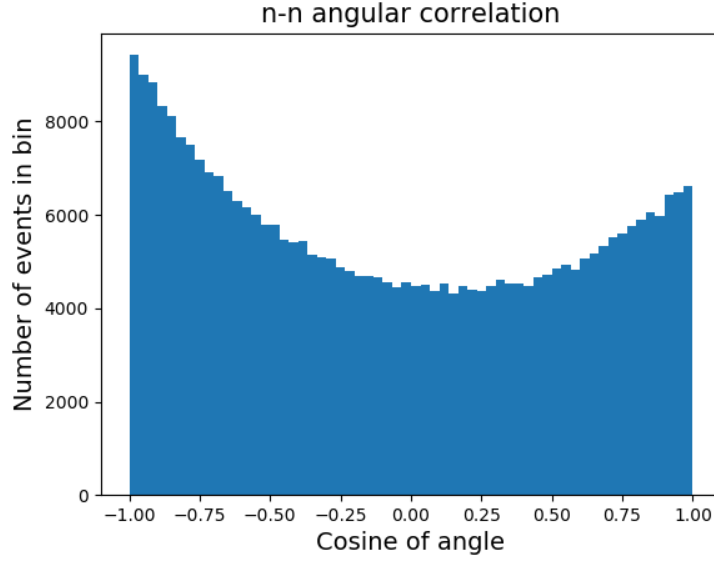
Figure 29: The angulare correlation between pairs of emmited neutrons from the neutron-induced fission of ^{239}Pu with $E_n = 0.1$ MeV
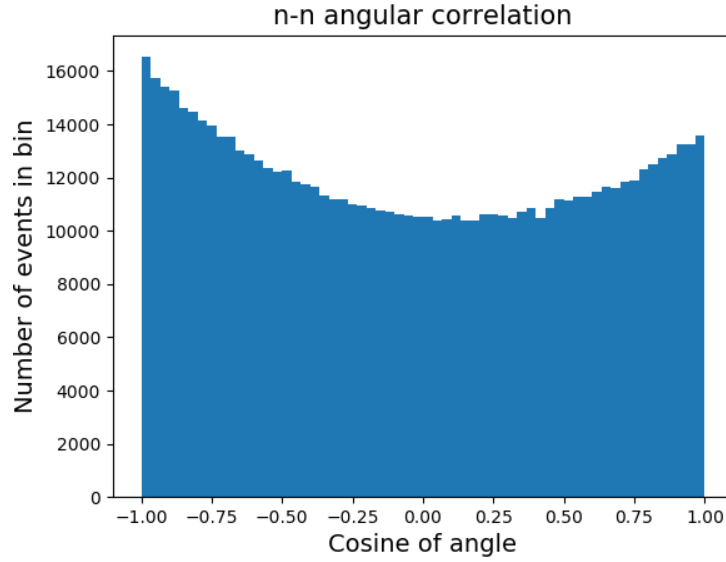

Figure 30: The angulare correlation between pairs of emmited neutrons from the neutron-induced fission of ^{239}Pu with $E_n = 8$ MeV
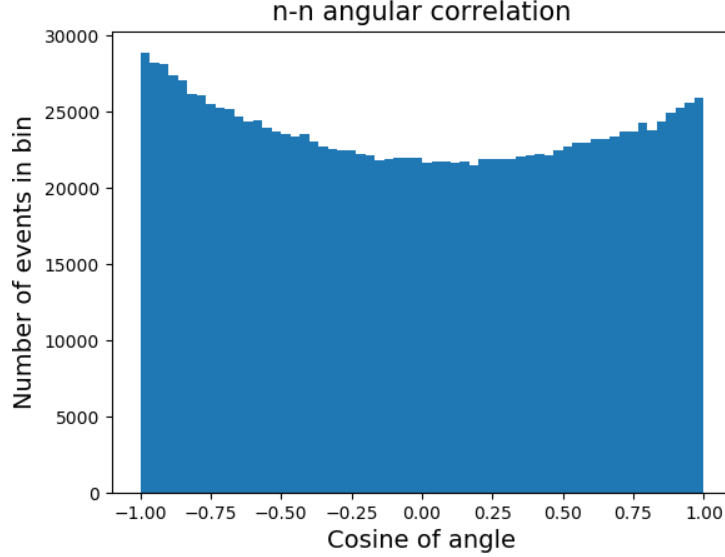
Figure 31: The angulare correlation between pairs of emmited neutrons from the neutron-induced fission of ^{239}Puwith $E_n = 20$ MeV

5 Discussion

From Table 2, I see that both the mean neutron multiplicity ν and the mean gamma multiplicity N_γ decreases as dTKE increases. As explained in section 2.1.1, dTKE decides how the available energy is partitioned between the kinetic energy and the excitation energy of the nucelus. As dTKE increases, less of the energy is put as excitation energy. As both neutron emission and gamma emission requires excitation energy from the nucleus, the average multiplicity of these decreases with increasing dTKE.

Furthermore, Table 3 shows that for higher x, the average neutron mutiplicity from the light fission fragment ν_1 increases, while the neutron muntiplicity from the heavy fission fragment ν_2 decreases. This is as expected. The parameter x shifts the distribution of excitation energy between the two fission fragments in the favour of the light fission fragment. The more excitation energy available, the more neutrons can the nucelus emit, as the nuceus must have more excitation energy than the neutron separation energy S_n to emit a neutron. Therefore, ν_1 increases while ν_2 decreases.

From Table 4, I see that the average gamma multiplicity N_γ increases as c_s increases. As explained in section 2.1.1, c_s is the so-called spin temperature, that effectively desides how much of the excitation energy should be rotational energy, compared to statistical excitation energy. As neutron emission more or less

25

conserves its own angular momentum during neutron emission, the total angular momentum of the nucleus remains unchanged, and thus neutron emission only strips the nucleus of statistical excitation energy. After neutron emission is no longer possible, the nucleus rids itself of rotational excitation energy through the emission of photons. Therefore, the more energy available as rotational excitation energy in the nucleus, the higher the average gamma multiplicity N_γ will be, and this is in accordance with Table 4.

As can be seen from Figure 14, 15 and 16, in neutron induced fission, the fragment mass distribution changes with the energy of the incoming energy. For low incoming neutron energies, the fission fragment distribution has two separate humps for low and high frament mass respectively, while for larger incomning neutron energies the two humps becomes more like a one hump distribution. The reason why, is that for low compound nucleus energies, shell effects play a large role in determining the fission fragments. When one of the fission fragments have neutron or proton numbers which correspond to magic numbers, where the nucleus is especially bound, more energy is released. For higher incoming neutron energies, however, the compound nucleus have a higher excitation energy, and therefore shell effects are less prominent. This can be seen when the two fission fragment distribution humps merge into one hump for large incoming neutron energies.

In Figure 29, 30 and 31, I observe that the angular correlation between pairs of emmited neutrons after neutron induced fission become less prominent for high incoming neutron energies. The neutrons are emmited in the fission fragment's rest system, and in this system, the neutrons are emitted isotropically. However, due to the kinetic energy of the fission fragment, the neutrons get a boost in the direction of the velocity of the fission fragments, when observed from the lab system. For lower energy neutrons, this boost is dominant, and as all the neutrons get this boost, there is a strong angular correlation between the emitted neutrons in the lab system. For higher incoming neutron energies, more excitation energy is availible when the neutrons are emmited, and the neutrons have a higher velocity. This velocity is not negligle comparet to the kinetic energy of the fission fragment, and thus the angular correlation between the emmited neutrons are less prominent.

From Figure 17, 18 and 19, I observe that the neutron multiplicity distribution changes for neutron-induced fission for different incoming neutron energies. For higher incoming neutron energies, more neutrons are emmited. This can also be seen in Table 6 - 10, where ν increases with incomig neutron energy. As explained earlier, this is due to more available excitation energies, such that the fission fragments can emit more neutrons before the excitation energy drops behow the neutron separation energy, and neutron emission is no longer possible. Furthermore, it can be seen that for low incoming neutron energies, few pre-fission neutrons are emmited from the compound nucleus, but several are emmited for higher energies. This is in accordance to what the FREYA user manual describes, as emission of neutrons from the pre-equilibrium nucelus only

contributes for higher energies.

From Figure 23, 24 and 25 one can also observe that the photon multiplicity distribution shifts to higher photon multiplicities for higher energies. As in the case for neutrons, higher excitation energy of the compound nucleus leaver more energy available for photon decay, and thus, we get on average a lager number of photons emmited per fission event.

From Figure 20, 21 and 22 can I see that the neutron spectral shape fits with a Boltzmann distribution for low incoming neutron energies, while for higher incoming neutron energies, the Boltzmann distribution only fits the spectral shape for low outgoing neutron energies. This means that thermal evaporation is a good model for neutron emission for low incoming neutron energies, as well as for high incoming and low outgoing neutron energies, but it no longer valid for high incoming and outgoing neutron energies.

6   Conclusion

In this report, I have studied the basics of FREYA to understand how the fission process is modelled. I have studied the effects of changing some key parameters, and found the effects in accordance to expectations. Furthermore, I have seen that FREYA reproduces theoretical expectations when the physical parameters of a fission events changes.

References

[1] R. Vogt J. M. Verbeke, J. Randrup. Freya user manual 2.0.2.

[2] Kenneth S. Krane. *Introductory Nuclear Physics*. John Wiley & Sons, 1988.

[3] Cyriel Wagemans. *The Nuclear Fission Process*. CRC Press, 1991.